Acta Pharmaceutica Sinica B 2019;9(5):960–972

Chinese Pharmaceutical Association
Institute of Materia Medica, Chinese Academy of Medical Sciences

Acta Pharmaceutica Sinica B

www.elsevier.com/locate/apsb
www.sciencedirect.com

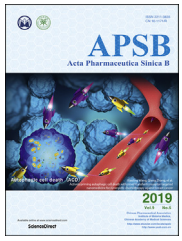

ORIGINAL ARTICLE

Improvement in affinity and thermostability of a fully human antibody against interleukin-17A by yeast-display technology and CDR grafting

Wei Sun[†], **Zhaona Yang**[†], **Heng Lin, Ming Liu, Chenxi Zhao, Xueying Hou, Zhuowei Hu, Bing Cui**[*]

State Key Laboratory of Bioactive Substance and Function of Natural Medicines, Institute of Materia Medica, Chinese Academy of Medical Sciences & Peking Union Medical College, Beijing 100050, China

Received 8 November 2018; received in revised form 24 November 2018; accepted 27 November 2018

KEY WORDS

Monoclonal antibody;
Antibody maturation;
Phage display;
Yeast surface display;
CDR grafting;
Antibody engineering

Abstract Monoclonal antibodies (mAbs) are widely used in many fields due to their high specificity and ability to recognize a broad range of antigens. IL-17A can induce a rapid inflammatory response both alone and synergistically with other proinflammatory cytokines. Accumulating evidence suggests that therapeutic intervention of IL-17A signaling offers an attractive treatment option for autoimmune diseases and cancer. Here, we present a combinatorial approach for optimizing the affinity and thermostability of a novel anti-hIL-17A antibody. From a large naïve phage-displayed library, we isolated the anti-IL-17A mAb 7H9 that can neutralize the effects of recombinant human IL-17A. However, the modest neutralization potency and poor thermostability limit its therapeutic applications. *In vitro* affinity optimization was then used to generate 8D3 by using yeast-displayed random mutagenesis libraries. This resulted in four key amino acid changes and provided an approximately 15-fold potency increase in a cell-based neutralization assay. Complementarity-determining regions (CDRs) of 8D3 were further grafted onto the stable framework of the huFv 4D5 to improve thermostability. The resulting hybrid antibody 9NT/S has superior stabilization and affinities beyond its original antibody. Human fibrosarcoma cell-based assays and *in vivo* analyses in mice indicated that the anti-IL-17A antibody 9NT/S efficiently

Abbreviations: AIN457, secukinumab; CDRs, complementarity-determining regions; FACS, fluorescent-activated cell sorting; HC, heavy chain; HRP, horse radish peroxidase; K_D, dissociation constant; K_{off}, the dissociation rate constant; K_{on}, the association rate constant; LC, light chain; LY2439821, ixekizumab; mAbs, monoclonal antibodies; MACS, magnetic-activated cell sorting; MFI, mean fluorescence intensity; scFv, single-chain variable fragment; VH, the variable regions of heavy chains; VL, the variable regions of light chains; YSD, yeast surface display

[*]Corresponding author. Tel./fax: +86 10 83165034.
E-mail address: cuibing@imm.ac.cn (Bing Cui).
[†]These authors made equal contributions to this work.

Peer review under responsibility of Institute of Materia Medica, Chinese Academy of Medical Sciences and Chinese Pharmaceutical Association.

https://doi.org/10.1016/j.apsb.2019.02.007

inhibited the secretion of IL-17A-induced proinflammatory cytokines. Therefore, this lead anti-IL-17A mAb might be used as a potential best-in-class candidate for treating IL-17A related diseases.

1. Introduction

IL-17A is a proinflammatory cytokine produced by the Th17 subset of T-cells[1]. Th17 cells are an identified subset of T helper cells associated with chronic inflammation, autoimmune disorders, fibrotic disease, and cancer[1–4]. Therefore, the development of IL-17A-targeted therapeutic agents has important clinical benefits[5]. Indeed, the anti-IL-17A antibodies secukinumab (AIN457), a human IgG1κ monoclonal antibody, and ixekizumab (LY2439821), a humanized IgG4 monoclonal antibody, have demonstrated significant effectiveness in treating these diseases, particularly psoriasis, psoriatic arthritis and ankylosing spondylitis[6,7]. Secukinumab or Ixekizumab prevents IL-17A from binding to its receptor and inhibits its ability to trigger inflammatory responses, which play a key role in the development of various diseases. Several agents targeting the IL-17A are currently under clinical trials as well. The ongoing studies focus on the efficacy of anti-IL-17 antibodies (*e.g.*, bimekizumab, ALX-0761, CJM112, CNTO 6785, and SCH-900117), nanoantibodies (*e.g.*, MSB0010841) and dual anti-IL-17/TNF-α inhibitors (*e.g.*, ABT-122, COVA322)[8,9]. Thus, IL-17A is an attractive target for intervention[5,10].

Monoclonal antibodies (mAbs), which constitute the main class of biotherapeutics, have been recognized as major medical tools for the treatment of multiple diseases in recent decades[11–14]. The success of antibody therapeutics has introduced competition in the development of novel therapeutic mAbs according to a first-in-class strategy for promising targets and a best-in-class strategy for clinically validated targets[15]. *In vitro* display technology, mAbs humanization, and human immunoglobulin transgenic mice have made it possible to obtain fully human mAbs[16]. Humanized antibodies or fully human antibodies not only have significantly reduced immunogenicity but also exhibit properties similar to those of human IgGs[17]. Display technology can rapidly separate specific mAbs with high affinities during optimization of the lead mAbs[18–20]. In the current study, we utilized several approaches to optimize anti-IL-17A antibodies with potential best-in-class candidates. We initially isolated a novel fully human monoclonal antibody to human IL-17A (Clone: 7H9) from a large naïve human phage-displayed scFv library. However, the modest neutralization potency limits its therapeutic applications. The current study presents our strategies to improve the binding affinity, stability and neutralization potency of 7H9. Both phage and yeast antibody displays are widely employed to increase antibody affinity *in vitro*[16,21]. The advantages of yeast over phage display include the ability to directly measure equilibrium dissociation constant (K_D) on the yeast surface and enrich high-affinity clones by flow cytometry without expression, purification, and characterization for a large number of different clones[16]. Therefore, the variable regions of 7H9 were randomized by error-prone PCR and high affinity clones were selected by yeast-displayed technology. Following analyses of residue substitutions by back-mutations and alanine scanning, we found an affinity-matured clone (Clone: 8D3) but it has low thermostability. It has been reported that properties such as stability and expression vary among particular families of V-genes. V-genes from the VH1, VH3 and VH5 families are better bio-therapeutic candidates than those from other families[22]. To improve the properties of these unstable V-genes, through a technique known as CDR grafting, the antigen-binding loops of a donor framework are transferred to an acceptor framework with known favorable properties[23]. Interestingly, through the above approaches, we have developed a CDR-grafted thermostable clone (Clone: 9NT/S) that exhibits improved binding and neutralization activities against IL-17A *in vitro* and *in vivo*. This leading antibody might act as a promising best-in-class drug candidate for treating IL-17A-related diseases.

2. Materials and methods

2.1. Cells, media, and plasmids

HT1080 cells were obtained from China National Infrastructure of Cell Line Resource (Beijing, China) and maintained at 37 °C, 5% CO_2, in Gibco MEM media (Thermo Fisher Scientific, Waltham, MA, USA) supplemented with 10% fetal bovine serum (Gibco), 2 mmol/L l-glutamine, 20 mmol/L HEPES buffer pH 7.3 and 1 × penicillin–streptomycin (Gibco). 293ET cells were purchased from Cell Resource Center, Institute of Basic Medical Sciences, Chinese Academy of Medical Sciences (Beijing, China). FreeStyle™ 293-F cells were obtained from Invitrogen (Carlsbad, CA, USA) and maintained as company instructions. *Saccharomyces cerevisiae* strains EBY100 (ATCC® MYA4941) was used for surface display. The vector pYD1(Addgene, Watertown, MA, USA) provided the backbone for all scFv surface-display experiments, while plasmid pFUSE-hIgG1-Fc2 (InvivoGen, San Diego, CA, USA) provided the backbone for scFv-Fc expression. The vector pFUSEss-CHIg-hG1, pFUSE2ss-CLIg-hk, and pFUSE2ss-CLIg-hL2 (InvivoGen) provided the backbone for human IgG1 expression. EBY100 was grown in YPD medium (10 g/L yeast extract, 20 g/L peptone, 20 g/L dextrose). SD-CAA (20 g/L dextrose, 6.7 g/L yeast nitrogenous base, 100 mmol/L sodium phosphate buffer pH 6.0 and 5.0 g/L bacto-casamino acids lacking tryptophan and uracil) and SG-CAA (20 g/L galactose, 6.7 g/L yeast nitrogenous base, 100 mmol/L sodium phosphate buffer pH 6.0 and 5.0 g/L bacto-casamino acids lacking tryptophan and uracil) medium was used for pYD1-transformed EBY100 and protein induction. *E. coli* DH5α (Transgen Biotech, Beijing, China) was used for subcloning and preparation of plasmid DNA. *E. coli* XL1-Blue (Transgen Biotech) was used to rescue and amplify phage. XL1-Blue was grown in SB medium (30 g/L tryptone, 20 g/L yeast extract, 10 g/L MOPS, 10 g/mL tetracycline, pH at 7.4).

2.2. Library selection using phage display

Phage display construction and selection were conducted as previously described[16]. The library was grown overnight at 30 °C in SB medium

supplemented with M13KO7 helper phage (NEB Ipswich, MA, USA), 100 μg/mL ampicillin, 50 μg/mL kanamycin and 10 μg/mL tetracycline. Phages were precipitated with a solution of PEG-8000 and NaCl to a concentration of 4% PEG-8000/3% NaCl followed by centrifugation at 12,000 rpm (Beckman Coulter, Brea, CA, USA). Phages were then resuspended in 1% (*w/v*) bovine serum albumin (BSA)/phosphate buffered saline (PBS). To select phages that bind to human IL-17A, recombinant phages were first pre-panned in an immunotube (Thermo Fisher Scientific, Waltham, MA, USA) coated with 4% (*w/v*) milk powder/PBS (pH 7.4), and subsequently transferred to another immunotube that had been coated with 2 μg/mL recombinant human IL-17A (PeproTech, Rocky Hill, NJ, USA) and blocked with 4% (*w/v*) milk powder/PBS (pH 7.4). Following a 2-h incubation, the tube was washed 5 times with PBS plus 0.1% Tween 20 (PBST) followed by 5 washes with PBS. Bound phages were then eluted by the addition of 1 mL glycine elution buffer (0.2 mol/L glycine-HCl, pH 2.2, 1 mg/mL BSA) for 10 min. The eluted phages were amplified by re-infection of *E. coli* XL1-blue, followed by three additional rounds of selection using 20 washes with PBST and 20 washes with PBS. Eluted phages from the fourth round of panning were used to re-infect *E. coli* XL1-blue, single clones expanded in 96 deep well plates and treated with helper phage using previously described methods[24]. Culture supernatants containing phage were used in ELISAs with plates coated with recombinant IL-17A or BSA, followed by washing with PBST. Bound phages were detected using anti-M13 antibody conjugated to horse radish peroxidase (HRP) (GE Healthcare, Chicago, IL, USA) at a 1:5000 dilution in 4% milk powder in PBS, followed by detection with 3,3′,5,5′-tetramethylbenzidine substrate. The reaction was stopped by the addition of 2 mol/L H_2SO_4 and recorded at 450 nm using an Infinite M200 plate reader (Tecan, Männedorf, Switzerland). The positive clones were sequenced and analyzed in IMGT website for the heavy chain and light chain genes (http://www.imgt.org/IMGT_vquest/vquest?livret = 0&Option = humanIg).

2.3. Protein expression in mammalian cells

IgGs were generated from scFv genes as described[25]. Briefly, VH genes were amplified using PCR and cloned into *Eco*RI- and *Nhe*I-digested pFUSEss-CHIg-hG1 vector. Similarly, VL genes were amplified, digested with *Eco*RI as well as *Bsiw*I and cloned into pFUSE2ss-CLIg-hk. For V gene cloning, pFUSE2ss-CLIg-hL2 vector and PCR products were digested with *Eco*RI and *Avr*II.

Recombinant antibodies were produced in Freestyle™ 293-F cells (Life Technology, Carlsbad, CA, USA) following transient transfection with 1 mg/mL DNA at a DNA/PEI ratio of 1:2.5 (PEI, Polyscience) as previously described[25]. Antibodies were purified from culture supernatants using protein G-Sepharose (GE Healthcare) and dialyzed against PBS. Purified antibodies were loaded onto a Hiload 16/600 Superdex 200 gel filtration column (GE Healthcare) to remove aggregates, followed by analyses of the 'monomeric' antibodies using Superdex™ 200 Increase 3.2/300 (GE Healthcare). Purified proteins were concentrated to 4 mg/mL by a 10 kDa Centrifugal Filter Unit (Millipore, Burlington, MA, USA), filtered by 0.22 μm Millipore filter.

2.4. Affinity measurements using surface plasmon resonance

Binding assays were carried out using biolayer interferometry (BLI) by Octet RED96 system (ForteBio, Fremont, CA, USA). All steps were performed at room temperature in a 96-well plate containing 200 μL per well. Streptavidin-coated biosensors were loaded with 5 μg/mL biotinylated recombinant human IL-17A (Sino Biological, Beijing, China) for 300 s followed by washing. The sensors were then reacted for 300 s with 100 nmol/L antibodies and then moved to buffer containing wells for another 300 s. Kinetic parameters were analyzed and compared using ForteBio Data Analysis (ForteBio).

A Biacore T100 instrument (GE Healthcare) was used for all kinetics measurements. The affinity of IL-17A binding to anti-IL-17A antibody variants was determined by surface plasmon resonance (SPR) measurements on a Biacore T100 instrument (GE Healthcare). All samples were in HBST buffer (10 mmol/L HEPES with 0.15 mol/L NaCl, 3.4 mmol/L EDTA, and 0.005% Tween-20, pH 7.2). A CM5 Chip was air-initialized and activated with EDC/S-NHS. Each of the anti-IL-17A antibody variants was diluted in acetate buffer (pH 5.5) and immobilized onto the chip. After blocking available unbound sites on the chip with ethanolamine, the chip was washed with HBST buffer and rotated. IL-17A was run at 25 mL/min for 300 s at various concentrations, then followed by a 10-min dissociation step. Binding parameters were determined with the Langmuir single binding site model using BIAcore T100 evaluation 2.0.3. (GE Healthcare).

2.5. Construction of mutant scFv yeast display libraries

The yeast display vector pYD1 was modified to allow scFv library construction by sequential cloning of antibody heavy (VH) and light (VL) chain gene repertoires (Supporting Information Fig. S3). The resulting vector (pYDs) used the GS linker between the VH and VL genes which were flanked by restriction enzyme sites for cloning the V-genes. The V5-tag and His6-tag were at the C-terminal of scFv in pYDs. The modified gene fragment was synthesized and cloned into the pYD1 backbone for scFv library construction and affinity maturation.

The gene encoding the 7H9 scFv was randomized using a GeneMorph II random mutagenesis kit (Stratagene, San Diego, CA, USA) to give a high mutagenesis rate. Primers were designed to PCR-amplify the VH gene or VL gene (Supporting Information Table S4) from pYDs-7H9 construct. After 5–7 rounds of error-prone PCR reactions, the mutated VH or VL scFv gene was gel-purified using gel extraction kit (Qiagen) and the resulting repertoire (10 μg) was cloned directly into Saccharomyces cerevisiae strain EBY100 by gap repair into 50 μg of digested pYDs, which created the 7H9 VH-Mut library or 7H9 VL-Mut library, respectively. Transformation mixes were subcultured in SDCAA. Library size was determined by plating serial dilutions of the transformation mixture on SDCAA plates. After subculturing, scFv display was induced by culturing in SGCAA medium for 48 h at room temperature. The VHVk-Mut library was also constructed by a similar approach. The VL mutant fragment was PCR-amplified and cloned directly into an AscI- and SaI- digested VH-Mut sub-library by gap repair.

2.6. Isolating candidate scFv clones using magnetic-activated cell sorting (MACS) and fluorescence-activated cell sorting (FACS)

An enrichment of the affinity-improved clones was performed as described previously[16]. Briefly, 2×10^9 yeast cells were used for this step. Biotinylated recombinant human IL-17A (Sino Biological) and 200 μL of streptavidin microbeads (Miltenyi Biotec, San Diego, CA, USA) were used for MACS to isolate antigen-specific scFvs. The eluted cells were grown in SDCAA medium and then induced in SGCAA. Alternatively, anti-biotin microbeads (Miltenyi Biotec) were used during successive MACS selections to decrease the enrichment of

clones that bound to the secondary reagent. After expansion, the MACS output cells were further enriched by FACS (BD Biosciences) using procedures and protocols similar to those described previously[16]. 2×10^8 cells were washed and resuspended in FACS buffer (1% BSA in PBS) and incubated with biotinylated recombinant human IL-17A. After incubation, cells were washed and incubated in FITC conjugated anti-V5 (1:1000, Abcam, Cambridge, UK) and APC conjugated Streptavidin (1:1000, ThermoFisher Scientific) for 1 h at 4 °C. The labeled cells were washed and sorted. Typically, the highest 0.1%–0.3% of the IL17A-binding population was gated in the sorting. Collected cells were grown in SDCAA medium and used for the next round of sorting after induction in SGCAA as described above. After the final round of sorting, 96 individual clones were picked, induced, and incubated with biotinylated recombinant human IL-17A, as detected by FITC conjugated anti-V5 and APC conjugated Streptavidin to identify the best candidates.

2.7. Measurement of yeast-displayed scFv affinity for IL17A

Quantitative equilibrium binding was determined using yeast displayed scFv and flow cytometry as described previously[16]. In brief, seven concentrations from 200 nmol/L to 1.56 nmol/L of biotinylated recombinant human IL-17A were used. Incubation volumes and the number of yeast cells stained were chosen to keep the number of antigen molecules in 10-fold excess above the number of scFv. The scFv-displaying yeasts were detected by FITC conjugated anti-V5 and APC conjugated Streptavidin. Finally, the yeasts were washed by cold FACS buffer and the mean fluorescence intensity (MFI) of IL17A binding was measured by flow cytometry. The MFI was plotted against the concentration of antigen and the K_D was determined by Eq. (1):

$$y = m1 + m2 \times m0/(m3 + m0) \quad (1)$$

where y is MFI at a given antigen concentration, $m0$ is antigen concentration, $m1$ is MFI of the no antigen control, $m2$ is MFI at saturation, and $m3$ is K_D. The equilibrium titration data were fit to a reversible binding model using Prism 5 Software (GraphPad Inc., San Diego, CA, USA) to determine the K_D.

2.8. Generation and rapid characterization of scFv-Fc fusions

In general, two extra digest sites, *Kpn*I and *Sal*I, were inserted into pFUSE-hIgG1-Fc2 between *Eco*RI and *Bgl*II to facilitate the rapid constructs transfer. DNA of pDYs-scFv was digested with *Kpn*I and *Sal*I and ligated into the modified pFUSE-hIgG1-Fc2. Vectors were used to transiently transfect 293ET cells. On the next day of transfection, the culture medium was changed to protein-free medium (Invitrogen). On the fifth day after transfection, supernatant containing IgG was collected, serially diluted with protein-free medium and mixed with 10 nmol/L recombinant human IL-17A (Peprotech) at room temperature for 1 h. Then these mixtures were incubated with HT1080 cell at 37 °C in 5% CO_2 for 24 h as described above. Measurement of IL-6 in culture supernatants was performed using human IL-6 ELISA kit (eBioscience, San Diego, CA, USA) according to manufacturer's description.

2.9. Antibody affinity measurements by ammonium thiocyanate assay

Estimation of the antibody affinity was performed by chaotropic ELISA using increasing concentrations of ammonium thiocyanate from in PBS-T as previously described[26]. Briefly, a constant 100 ng on hIL-17A was coated onto plates overnight. After blocking, antibody incubating and washing, increasing concentrations of ammonium thiocyanate from 0 to 3.5 mol/L were added to the wells. After 10 to 15 min, the plates were washed and the remaining antibody was detected by ELISA.

2.10. ELISA assay for IL-17A binding

96-well Costar ELISA plates (Corning Inc., Corning, NY, USA) were coated with 100 µL of 1 µg/mL human IL-17A (PeproTech) in PBS over night at 4 °C. The plates were blocked for 2 h with blocking buffer (PBS containing 4% skimmed milk powder), followed by washing four times with PBS containing 0.1% Tween20. Next, titrated amounts of purified antibody variants diluted in blocking buffer were added to the plates and incubated for 1 h. Following washing, bound protein was detected using HRP conjugated goat-anti-human IgG antibodies (CWBIO, Cambridge, MA, USA) at a 1:8000 dilution in blocking buffer, followed by detection with 3,3′,5,5′-tetramethylbenzidine substrate. The reaction was stopped by the addition of 2 mol/L H_2SO_4 and recorded at 450 nm using a Tecan Infinite M200 plate reader.

2.11. Protein thermostability by ELISA

The purified antibodies were diluted in PBS with 1% BSA to a final concentration of 1 mg/mL. The variants were then incubated for 30 min at different temperatures ranging from 37 to 100 °C by a thermal cycler (Bio-Rad, Hercules, CA, USA). The reaction was terminated by flash freezing the proteins in liquid nitrogen. The proteins were held at –80 °C and then were tested the bindings to human IL-17A in ELISA. Determination of IC_{50} values was calculated using Prism curve fitting software (GraphPad Inc.).

2.12. Protein thermostability by differential scanning calorimetry

Thermal unfolding profiles of anti-IL-17A antibody variants were measured by differential scanning calorimetry (DSC) using a VP-Capillary DSC system (GE Healthcare)[27]. All antibodies were tested in PBS (pH 7.4) at protein concentrations ranging from 0.7–1.0 mg/mL at a scan rate of 1 °C/min. Samples were heated from 20 to 100 °C. Data analysis was performed using Origin 7 software (Originlab, Northampton, MA, USA). Transition midpoint values (T_m) were determined from the thermogram data using a non-two-state model which employs the Levenberg–Marquardt non-linear least-square method. Total calorimetric heat change values (ΔH) were determined by calculating the total area under a given antibody thermogram. The Fab transitions generally had CPmax values (*i.e.*, the height of a DSC peak) approximately three-fold greater than that of the CH2 or CH3 domains.

2.13. Fibroblast-based assay to assess the inhibition of IL-17-Induced IL-6 secretion

To determine the neutralization of anti-IL-17 antibodies, IgG activity was evaluated in an HT1080 human fibrosarcoma cell assay. These cells respond to human IL-17 by releasing IL-6 in a dose dependent manner. HT1080 cells were seeded in 96-well flat-bottomed tissue culture assay plates (Corning Inc.) at 5×10^4

cells/well. The purified IgGs were serially diluted (from 0 to 1350 nmol/L) in PBS and pre-incubated with recombinant human IL-17A (10 nmol/L final concentration) in assay media for 30–60 min at 37 °C. Media was aspirated from cells and 100 μL/well of assay media added and incubated overnight (18 ± 4 h). Supernatants were harvested and either assayed immediately or stored at –20 °C. IL-6 levels in supernatants were determined using human IL-6 ELISA kits (eBioscience) according to manufacturer's description. Determination of IC_{50} values was calculated using Prism curve fitting software (Graphpad).

2.14. *In vivo experiments in mice*

All experiments using animals were performed in accordance with protocols approved by the Animal Experimentation Ethics Committee of the Chinese Academy of Medical Sciences (Beijing, China), and all procedures were conducted in accordance with the guidelines of the Institutional Animal Care and Use Committees of the Chinese Academy of Medical Sciences (Beijing, China). All animal procedures were consistent with the ARRIVE guidelines. BALB/c female 8-week-old mice were put in quarantine for 3 weeks. At the age of 11 weeks, the mice were separated into four treatment groups (five mice per group). 200 μL PBS or the anti-IL-17A antibody variants (2 mg/kg) were pre-incubated for 20 min at room temperature with 200 μL human IL-17A (1.5 mg/kg, PeproTech). Treatment involved two subcutaneous conjugates injections in the flank area (400 μL/mouse). Two hours after injection, orbital venous sinus blood samples were collected. Sera were then separated and measured to determine the level of murine Gro-α with an ELISA kit (R&D Systems, Minneapolis, MN, USA) according to the manufacturer's instructions.

2.15. *Statistical analysis*

Data are shown as mean ± standard error of the mean (SEM), unless otherwise indicated. Multiple groups comparisons were analyzed by one-way ANOVA followed by Duncan's test in Prism 5 (GraphPad Inc.). $P < 0.05$ was considered statistically significant.

3. Results

3.1. *Isolation of antibodies to human IL-17A from a large naive phage-displayed scFv library*

A large naive scFv antibody library was prepared and maintained as previously described by our laboratory[24]. The primary library has approximately 3.7×10^8 transformants. After infecting Cre recombinase-expressing bacteria with the primary library, the light and heavy chain genes of the variable region (VL and VH) exchanged and their diversity exponentially increased[28]. The effective library sizes should be $\sim 1.7 \times 10^{11}$, and 80% of VH/VL DNAs have full length open reading frames without stop codons.

This phage-displayed scFv library was used for selection against recombinant human IL17A. After four rounds of panning, specific phages were enriched toward the antigen and monitored by phage ELISA. Phage scFvs that showed at least five-fold higher signals than the control values in the phage ELISA were preliminarily identified as positive clones (Fig. 1A). These positive binders were sequenced and assigned according to the IMGT database (http://www.imgt.org). The sequence data revealed 45 completely different anti-IL-17A scFv clones (Supporting Information Table S1). We did not find any scFv clone with identical or similar CDRs sequences to those of clinical anti-IL-17A antibody AIN457 or LY2439821 (Supporting Information Fig. S1). The heavy chain VH1 (16/45, 35.5%) and VH6 (20/45, 44.4%) gene segments were found to be the most frequent among the analyzed human VH sequences, followed by the VH3 (9/45, 20%) gene family. Within the human V-gene light chain sequences, Vλ3 gene family (23/45) constituted 51.1% of all analyzed sequences, followed by Vκ1 (6/45, 13.3%), Vκ2 (2/45, 4.4%), Vκ3 (4/45, 8.9%), Vλ1 (6/45, 13.3%), and Vλ2 (4/45, 8.9%) (Fig. 1B). These results indicate that most of the dominant germline families were represented in the leads generated after panning.

To rapidly validate these distinct phage clones through *in vitro* neutralization assay, genes of scFv fragments were transferred from phagemids to a vector encoding an Fc-fusion cassette. The mammalian expression vector, pFUSE2-scFv-Fc allows the rapid transient expression of the scFv gene as scFv-Fc fusions. The cell culture supernatants of all 45 distinct scFv-Fc fusions were collected, serially diluted and pre-mixed with 10 nmol/L recombinant human IL-17A. The IL-17A-containing supernatants were then used to stimulate HT-1080 cells to produce IL-6[29]. The results showed that at least 12 scFv-Fc fusions (7A8, 7C12, 7A4, 7G11, 7B6, 7H9, 7A6, 7F4, 7G11, 7H8, 7F10 and 7F1) had potential neutralizing effects (Fig. 1C and Supporting Information Fig. S2). To further narrow the range of the candidate antibody pool, the relative affinity of the antibody was measured by ammonium thiocyanate assays[30]. We found that 7A6,

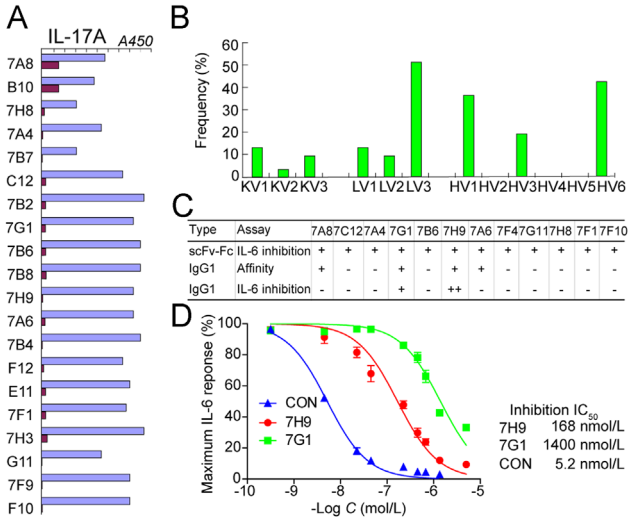

Figure 1 Selection of anti-IL-17A monoclonal antibodies (mAbs) from a phage-displayed scFv library. (A) Phage clones were isolated with the binding activity specific to IL-17A (blue bars), and low or no binding to BSA (brown bars) in phage ELISA. (B) Antibody gene family distribution and frequency of 45 phage clones analyzed by IMGT (http://www.imgt.org). (C) Summary of the antibody IL-6 inhibition and IL-17A binding activities. Antibodies selected from the phage-displayed library were converted into scFc-Fc or full-length IgG1 format. The summary data correspond with the results in Supporting Information Table S2, Fig. S2 and panel D. +, increase; ++, strong increase; –, no effect. (D) IL-6 inhibition curves of 7H9, 7G1 and AIN457 (CON) in IgG1 format. HT1080 cells were treated in triplicate with antibodies pre-mixed with 10 nmol/L IL-17A and IL-6 levels determined by ELISA. Data are shown as the mean ± SD ($n = 3$). IC_{50} was calculated using GraphPad Prism 5.0.

7A8, 7H9, and 7G1 scFv-Fc fusions had relatively higher binding affinity than the others (Supporting Information Table S2).

These four scFvs, as well as AIN457, were then converted into IgG1 by cloning the scFv variable regions into vectors encoding human IgG1 HC and LC (κ or λ) vectors. Antibodies were purified and assessed by SDS-PAGE and HPLC (data not shown), and then serially diluted to measure their neutralization activity. The results show that 7H9 and 7G1 are able to mildly inhibit IL-6 production in HT1080 cells (Fig. 1D), but 7A6 and 7A8 in IgG1 format have no blocking effect (Fig. 1C). The calculated IC50 values of 7H9 (166 nmol/L) and 7G1 (1392 nmol/L) for IL-17A inhibition were higher than that of the reference antibody AIN457 (5.2 nmol/L). Furthermore, we analyzed the binding behaviors of 7H9 and AIN457 over recombinant human IL-17A by surface plasmon resonance[18]. The association rate constant (K_{on}) of 7H9 is ~16-fold faster than that of the reference antibody AIN457, while the dissociation rate constant (K_{off}) is ~400-fold faster than that of AIN457, resulting in the decreased K_D binding behavior in general (Table 3). K_{off} is known to be an important parameter and have a significant correlation with neutralization measures[31,32]. These results suggest that affinity to IL-17A is a major determinant of neutralization by 7H9, which indicates that performing affinity maturation, especially slower K_{off}, might be a plausible way to improve neutralization.

3.2. *Enrichment of high-affinity mAbs using yeast surface display*

A YSD approach was employed to achieve affinity maturation. First, the 7H9 scFv gene was sub-cloned into the expression vector pYDs (Supporting Information Fig. S3) for YSD. To improve the contribution of VH or VL to affinity and neutralization, we separately mutated VH and VL in two different libraries. The 7H9 VH fragment gene was randomly mutated using error-prone PCR. The resulting repertoire was directly cloned into pYD1–7H9-scFv. This step resulted in a 7H9 VH-Mut (mutant) library containing 2.2×10^6 transformants. A 7H9 VL-Mut library with 1.9×10^6 transformants was generated using similar methods (Fig. 2A).

Two rounds of enrichment were carried out on magnetic bead columns[16,32]. In the first round, we used 100 nmol/L biotinylated IL-17A and streptavidin-magnetic microbeads to capture the bound yeast. In the subsequent round of MACS, we used the same concentration of biotinylated IL-17A but altered the microbeads to anti-biotin magnetic microbeads. The output was subjected to one more round of sorting on FACS by gating the highest 0.1%–0.3% binders against 100 nmol/L biotin-IL-17A (Fig. 2B). Following two rounds of MACS plus one round of FACS enrichment, the third mutation yeast library was constructed (Fig. 2A). The output of the 7H9 VH-Mut and 7H9 VL-Mut libraries generated after the first round of FACS enrichment provided mutants with abundant diversity and improved affinity (Fig. 2B). The output plasmid pool was extracted from yeast and transfected into *E. coli*. Afterwards, the VL mutant fragments were PCR-amplified and cloned directly into the digested VH-Mut sub-library resulting in the VHVL-Mut library. This library was subjected to three rounds of FACS selection using decreasing concentrations of biotinylated IL-17A varying from 50 to 5 nmol/L (Fig. 2B). From the output of the last round of FACS enrichment, we identified nine more distinct clones, which showed the higher biotinylated IL-17A-binding values in monoclonal screening (Fig. 3A). The K_D improvement of each affinity-matured clone was measured by flow cytometry with the purified biotinylated IL-17A compared with the original clone 7H9. The data show that the K_Ds of all the affinity-matured clones were higher than that of 7H9 (Fig. 3B). The best clone, 8D3, showed a 10.3-fold increase in binding (Fig. 3C).

For functional characterization, we converted these scFvs to full-length IgG1 format. The K_Ds for each IgG were determined using surface plasmon resonance. Compared with 7H9, the clone 8D3 displayed ~16-fold improvement in K_{off}, with a total ~30-fold improvement in K_D by Octet Fortebio (Table 1), while ~233-fold in K_{off} with a total ~8-fold in K_D by Biacore (Table 3). The neutralization of 8D3 has a 15-fold improvement over 7H9 (Table 1). However, 8D3 showed worse thermostability measured

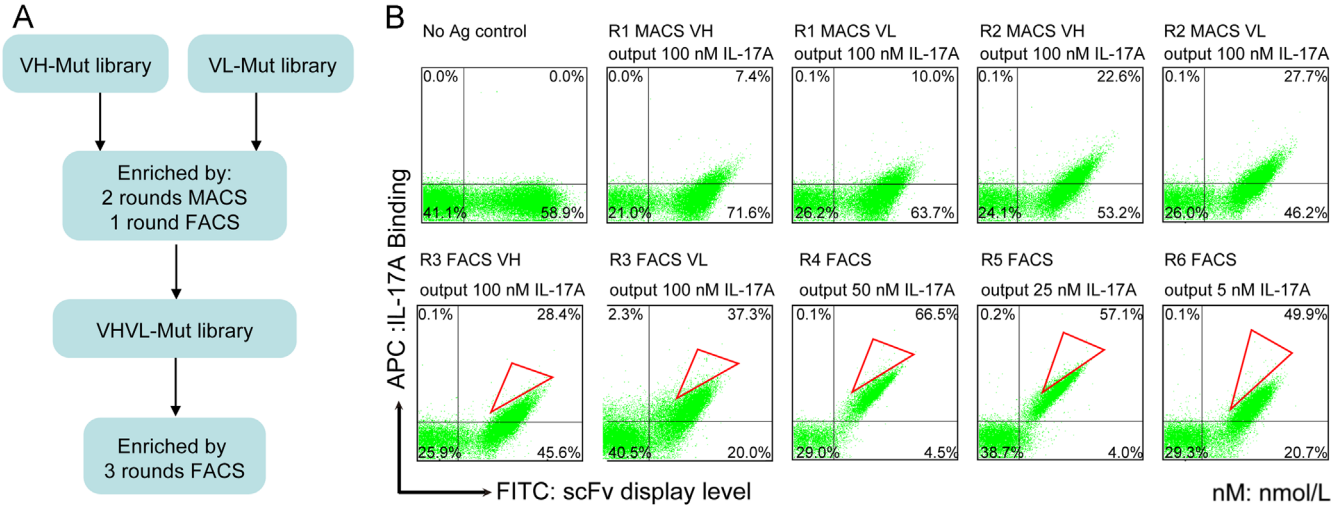

Figure 2 Enrichment of high-affinity mAbs using yeast surface display. (A) Technical scheme. The heavy chain random mutation (VH-Mut) library and the light chain random mutation (VL-Mut) library were constructed. After two rounds of magnetic bead screening (MACS) and one round of flow sorting (FACS), yeast clones with improved affinity were obtained. The heavy and light chains of these clones were recombined, and high-affinity clones were subsequently screened by three-round flow sorting. (B) Flow cytometry analysis of two-round MACS and four-round FACS sorting. The horizontal axis (*x*-axis, FITC channel) represents the expression level of the scFvs in the yeast cell population. The vertical axis (*y*-axis, APC channel) represents the level of the antigen, IL-17A, bound to the antibody. After two rounds of MACS sorting, FACS was performed to select the top 0.1%–0.3% populations with the strongest fluorescence intensity.

by DSC with a Fab melting temperature (T_m) value of 59.4 °C than that of its original clone 7H9 with a T_m value of 66.8 °C (Table 3). These results suggest that 8D3 has low thermostability, though it has been affinity-matured.

3.3. *Identification of the critical residues for antigen-antibody interaction*

The residues which were mutated and selected through yeast-displayed random mutagenesis contributed to antibody affinity maturation. Three residues (L30G, L70S and L92aV) were evolved in 8D3 light chain, and six residues (H15P, H35D, H65N, H83S, H93V and H97D) in 8D3 heavy chain compared to those in 7H9 (Fig. 4). To assess which residues play the key role, we individually mutated them back to their original residues. We found five back-mutations ($L70^{S\text{-}T}$, $L92a^{V\text{-}D}$, $H15^{P\text{-}S}$, $H35^{D\text{-}N}$ and $H83^{S\text{-}T}$) that had no or low effects on the antibody affinity measured with an ammonium thiocyanate assay. However, four mutants ($L30^{G\text{-}S}$, $H65^{N\text{-}S}$, $H93^{V\text{-}A}$ and $H97^{D\text{-}E}$) significantly lost their antigen bindings (Supporting Information Table S3). These

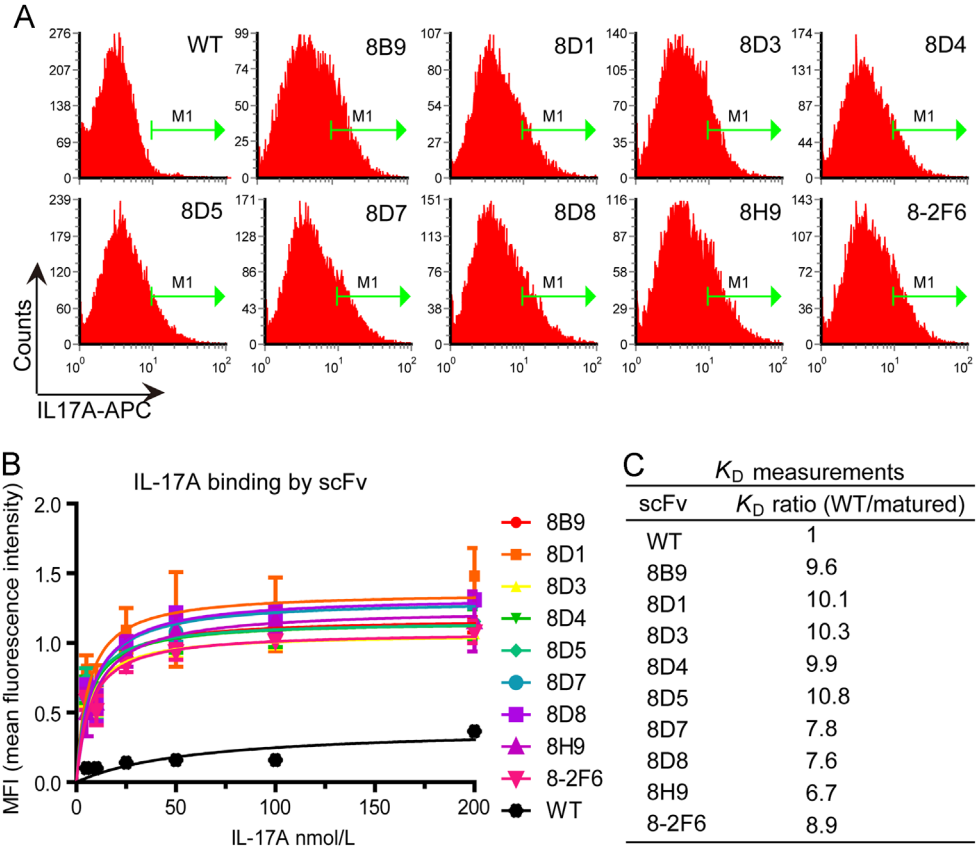

Figure 3 Identification of high-affinity mAb clones by flow cytometry. (A) Antibody clones were obtained after the third round of flow sorting. Flow cytometry analysis was performed to analyze the ability of the antibody to bind 10 nmol/L IL-17A. The horizontal axis (*x*-axis, APC channel) represents the level of the IL-17A antigen bound to the scFv antibody. (B) and (C) Mean fluorescence intensity (MFI, B) and affinity improvement (K_D ratio, C) assessed by the MFI values of wild type (7H9) and mutants in scFv formats on the yeast surface. Data are shown as the mean ± SD ($n = 3$).

Table 1 Summary of the antibody affinity measurement by Octet Fortebio and IL-6 inhibition activity in IL-17A-stimulated HT1080 cells.

Mutant	K_{on} (L/mol·s)	K_{off} (s^{-1})	K_D (mol/L)	IC_{50} (nmol/L)
WT (7H9)	2.35×10^4	1.66×10^{-3}	7.06×10^{-8}	166
CON	6.47×10^4	4.87×10^{-5}	7.53×10^{-10}	5
8D3	4.43×10^4	1.04×10^{-4}	2.34×10^{-9}	11
8D4	6.02×10^4	1.98×10^{-4}	3.29×10^{-9}	17
8-2F6	2.92×10^4	1.12×10^{-4}	3.82×10^{-9}	16
8B9	3.93×10^4	2.40×10^{-4}	6.10×10^{-9}	21
8D7	5.41×10^4	2.40×10^{-4}	4.43×10^{-9}	28

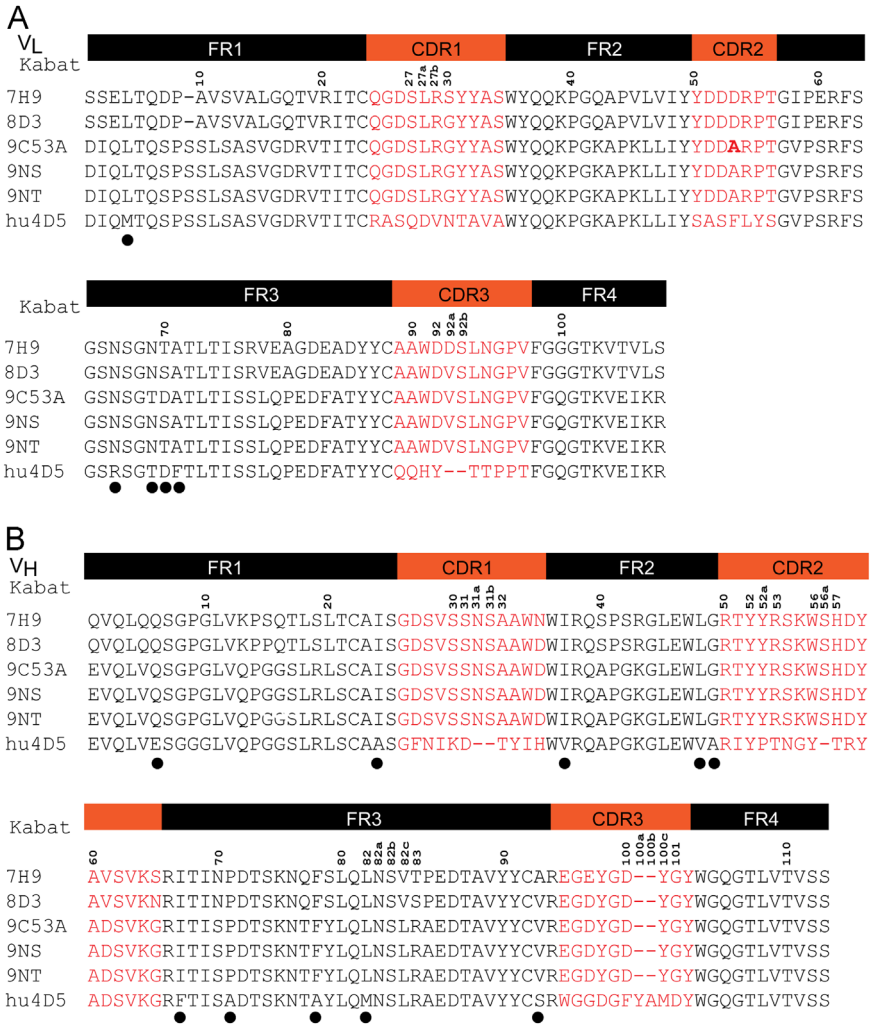

Figure 4 Multiple sequence alignment of relevant sequences. (A) The light chain variable domain (VL). (B) The heavy chain variable domain (VH). CDR residues are colored in red. Sequences were aligned by using the Clustal Omega program. Residue labels and CDR definitions are according to Kabat (1987). (●) indicates these residues were retained after CDR grafting onto the 4D5 framework.

results show that L30G in CDRL1, H65N in CDRH2, and H97D in CDRH3 are responsible for the improvement of antibody affinity, consistent with that CDRs are the major relevant sites for antigen binding[33]. Moreover, if H94 alanine of 7H9 structurally close to or in CDRH3 region is replaced by valine, an aliphatic hydrophobic amino acid, which might affect the conformation of the binding loop and ameliorate the antigen binding.

To further investigate the critical residues for antigen-antibody interactions, alanine scanning mutagenesis was carried out in both CDRs of heavy and light chains[34]. Each CDR non-alanine residue in 8D3 was mutated to alanine by site-directed mutagenesis. The effects of these mutations were assessed through analyzing the binding activity of purified IgG1 proteins with an ammonium thiocyanate assay. Unexpectedly, one mutation ($L53^{D-A}$) was able to enhance the binding (Table 2). These results indicate that residues that have lost their bindings are functionally critical for antigen-antibody interactions (Table 2); these results are also consistent with the previous analyses of back mutations. Four alanine substitutions ($L30^{G-A}$, $H65^{N-A,}$ $H93^{V-A}$ and $H97^{D-A}$) are harmful to their interactions with antigen (Table 2).

3.4. *Thermostability improvement through CDR grafting*

Given that the antibody 8D3 was not sufficiently stable, we improved its stability by grafting its binding residues onto the framework of the huFv 4D5 (simply denoted here by "4D5"). CDR grafts have primarily been introduced to reduce the immunogenicity of murine antibodies used in human *in vivo* applications. CDR grafting can also be used to improve the biophysical properties of antibodies by grafting their antigen specificities to a framework with better biophysical properties[23,35,36]. The CDRs are usually grafted onto the 4D5-framework, leading to a significant improvement of both expression yield and thermodynamic stability[36,37]. The 4D5 framework consists of a VH that is essentially identical to the germ-line IGHV 3–66 (IMGT nomenclature)[38] and the Vκ derived from germ-line IGKV 1–39 (IMGT nomenclature)[38], while the 8D3 framework is the same as its parent clone 7H9 framework, which is derived from the germ-lines IGHV 6-1(IMGT nomenclature) and germ-IGLV3–19 (IMGT nomenclature) (Supporting Information Table S1)[38]. It has been reported that antibodies with the HV 6 framework show poorly stability and expression[22]. Based on these conditions, we built a homology model of 8D3 and compared it to

Table 2 Alanine scanning mutagenesis of 8D3. The binding affinity of 8D3 alanine mutants was evaluated relative to the wild type 8D3 by ELISA.

L1/H1 residues	Effect	L2/H2 residues	Effect	L3/H3 residues	Effect
LD26	+/–	LY50	–	LW91	– – –
LS27	+/–	LD51	– –	LD92	– – –
LL28	– –	LD52	+/–	LV93	–
LR29	+/–	LD53	+	LS94	– –
LG30	–	LR54	– –	LL95	– –
LY31	+/–	LT56	+/–	LG95b	– –
LY32	–	HR50	– –	LV97	– – –
LS34	+/–	HT51	– –	HE95	– – –
HG26	– –	HY52	– –	HG96	– – –
HD27	– –	HS53	+/–	HD97A	+/–
HV29	– –	HK54	+/–	HY98	– –
HS31	– –	HS56	–	HG99	– – –
HS31b	– –	HH57	+/–	HD100	– – –
HD35	– –	HD58	–	HY100a	– – –
		HY59	– –	HG101	+/–
		HV61	+/–	HV100A	– –
		HS62	+/–	HD104E	– –
		HK64	+/–		
		HN65	–		

+, increase; +/–, moderate increase or no change; –, reduction; – –/– – –, significant reduction.

the X-ray structure of the human 4D5 version 8 Fv fragment (PDB entry 1fvc) (Fig. 5A)[39]. In VH and VL domains, in addition to CDR residues, several residues in the 'outer loop' of VH and VL, which are sometimes referred to as CDR4, are usually considered in studies (residues H69, H71, H75-H77, and L66-L71). These "outer loops" maintain the conformation and play a role in antigen binding. For example, residue L66 is usually Gly in κ light chains and assumes a positive Φ angle. If this residue is replaced by a non-Gly residue (Arg in 4D5), the outer loop assumes a different conformation, bending away from the upper core domain[23,36].

In VH domains, substitutions of residue H6, H67 and H82 can have a drastic effect on stability and potentially on antigen affinity as these residues determine the conformation of the framework[36] (Fig. 5B). In Vκ domains, residue L4 of the N-terminus (Leu in 8D3 and 7H9) packs together with certain residues of CDR-L1, CDR-L2, the outer loop, and CDR-L3 to form the upper core domain[23] (Fig. 5C). Additionally, certain residues (H24I, H37I, H48L, and H93V), which are in proximity to CDR regions, were retained to support their CDR structures (Fig. 5B). The necessity of H93V has been confirmed as described above, and it cannot be replaced. To further optimize the affinity, the mutation ($L53^{D-A}$) was also included (Fig. 5C). To determine the extent to which the "outer loop" of the light chain affects the functionality of a loop graft, 9C53A CDRs are on the hybrid 4D5 framework with the 4D5 "outer loop" of the light chain, while clones 9NT or 9NS with the 7H9 or 8D3 light chain "outer loop". In addition, the homology models of 8D3 and 9NT were aligned and analyzed in PyMOL (Fig. 5D). This was done by looking at the structural similarity of 8D3 *versus* 9NT, particularly in the CDR regions. Thus, the 8D3 CDRs were grafted on the 4D5-framework through total gene synthesis and a series of mutants were generated (Fig. 4).

To characterize these mutants, 9C53A, 9NS and 9NT were converted into full-length IgG1. They showed no detectable aggregation and degradation (Fig. 6A). Compared with their

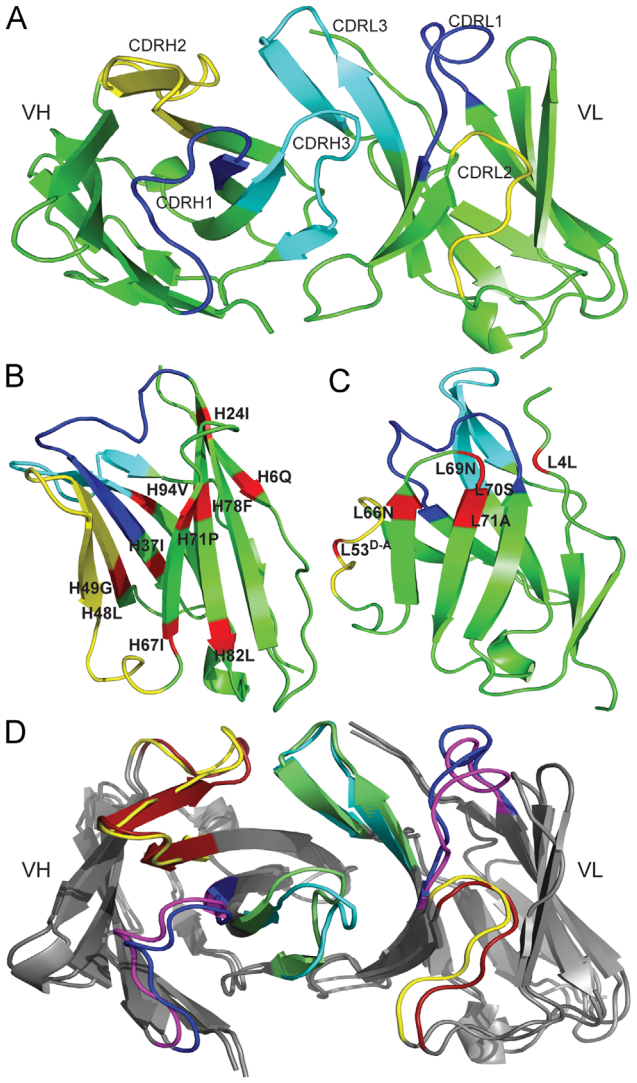

Figure 5 Structural analysis of 8D3 and 9NT variable regions. (A) Structural homology model of 8D3 variable regions. CDR1, CDR2 and CDR3 are shown in blue, yellow and cyan, respectively. (B) and (C) Structural homology model of 8D3 heavy chain variable domain (VH, B) and light chain variable domain (VL, C). CDR1, CDR2 and CDR3 are shown in blue, yellow and cyan, respectively. Framework residues in red were retained, and light chain 53 aspartates were replaced by alanine after CDR grafting on 4D5. (D) The variable regions of 8D3 and 9NT were aligned using the CDR residues. Here, only the CDR residues are shown in color. CDR1, CDR2 and CDR3 of 8D3 are shown in blue, yellow and cyan, respectively. CDR1, CDR2 and CDR3 of 9NT are shown in purple, red and green, respectively. The homology model of the antibody Fv structure was built through the ROSIE web server (http://rosie.rosettacommons.org/) and analyzed in PyMOL[39].

parent clone 8D3, 9C53A exhibited slight improvement in K_D but great increase in the Fab T_m value from 59.4 to 76.3 °C by DSC (Fig. 6B, C, and Table 3). 9NT and 9NS showed high affinity (2.81×10^{-10} mol/L for 9NT, 2.91×10^{-10} mol/L for 9NS). 9NS and 9NT displayed ~1.7-fold improvements in K_{off} relative to that of 8D3 (Table 3, and Supporting Information Fig. S4). The Fab T_m values of both 9NS (76.7 °C) and 9NT (77.4 °C) were close to that of 9C53A (76.3 °C) and ~18 °C higher than that of 8D3 (59.4 °C)

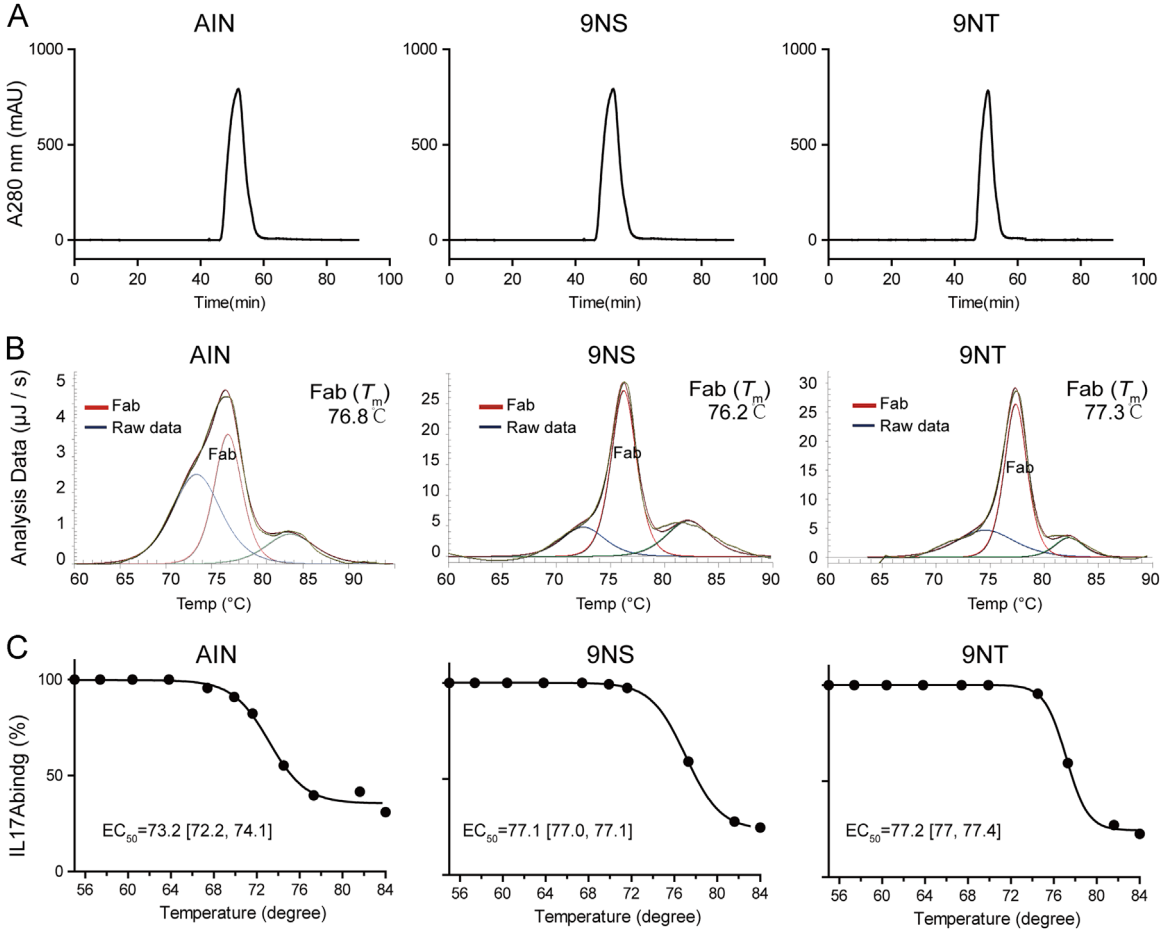

Figure 6 Characterization of the selected anti-IL-17A antibodies 9NT and 9NS. (A) Gel filtration chromatography analysis of purified antibodies. (B) and (C) Thermostability analysis of purified antibodies measured by DSC (B) and thermo gradients (C). The EC_{50} values and 95% confidence intervals are indicated on the bottom.

Table 3 Summary of the antibody affinities measured by Biacore T100 and thermostabilities by DSC.

Antibody variant	Biacore K_D (mol/L) (K_{on} (L/mol · s), K_{off} (s^{-1}))	Fab T_M (°C)
7H9 (WT)	3.56×10^{-9} (7.74×10^{6}, 6.00×10^{-2})	66.8
8D3	4.67×10^{-10} (5.51×10^{5}, 2.58×10^{-4})	59.4
9C53A	3.35×10^{-10} (5.36×10^{5}, 1.79×10^{-4})	76.3
9NS	2.91×10^{-10} (5.91×10^{5}, 1.72×10^{-4})	76.7
9NT	2.81×10^{-10} (5.34×10^{5}, 1.50×10^{-4})	77.4
AIN457	3.23×10^{-10} (4.71×10^{5}, 1.52×10^{-4})	76.8

by DSC. Furthermore, their stabilities were measured with AIN457 through thermal gradients. In this assay, full-length IgG1 9NS and 9NT showed 5 °C higher thermal tolerance than AIN457 (Fig. 6C). Generally, 9NS and 9NT behave similarly in affinity and thermostability assays. These results suggest that "outer loops" maintain the antibody conformation and CDR grafting benefits the affinity and thermostability of antibodies.

3.5. Cell-based assay and in vivo analysis of optimized anti-IL-17A antibodies

To investigate the neutralizing ability of the anti-IL-17A antibodies, antibodies were tested in a neutralization assay. The results showed that both 9NS and 9NT were able to inhibit IL-6 production in a similar manner as the reference antibody AIN457 in HT1080 cells. The calculated IC_{50} values of 9NS (10.5 nmol/L) and 9NT (9.2 nmol/L) for IL-17A inhibition were slightly better than that of AIN457 (15.6 nmol/L) (Fig. 7A). Generally, approximately 20 ng/mL 9NS or 9NT was sufficient to inhibit 10 nmol/L IL-17A-induced IL-6 secretion in HT1080 (Fig. 7A). Here, 9NS and 9NT function similarly and are viewed as the same clone (simply denoted here by "9NT/S"). Because 9NT specifically bound to human IL-17A without cross-reaction with other IL-17 family cytokines or mouse IL-17A (Supporting Information Fig. S5), recombinant human IL-17A was employed in the following experiments. To further examine the *in vivo*

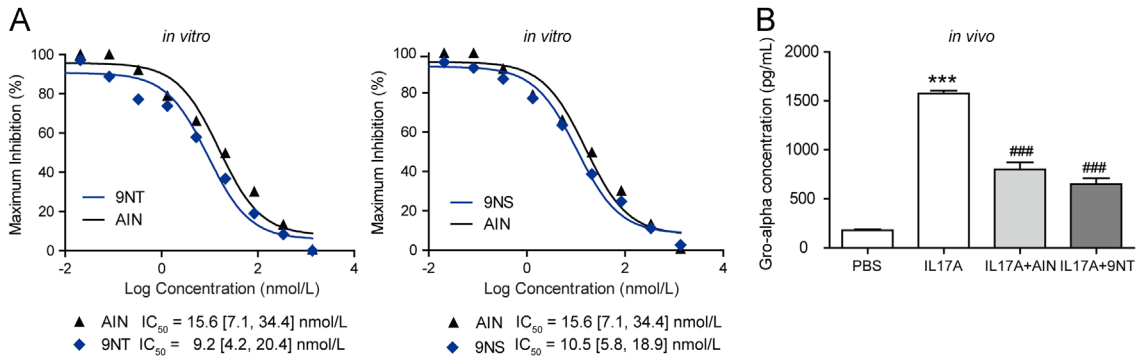

Figure 7 The *in vitro* and *in vivo* activity of the selected anti-IL-17A antibodies 9NT and 9NS. (A) The IL-6 inhibition effects of anti-IL-17 antibodies in IL-17A-stimulated HT1080 cells *in vitro*. The IC_{50} values and 95% confidence intervals are indicated on the bottom. (B) The serum Gro-α concentration were tested by ELISA from the mice injected with PBS or with IL-17A (1.5 mg/kg). Pre-incubation of IL-17A with anti-IL17A antibody (2 mg/kg), 9NT inhibited Gro-α secretion. Data are shown as the mean $\pm$ SEM; $^{***}P < 0.001$ compared with the PBS group; $^{###}P < 0.001$ compared with the IL-17A group.

inhibitory activity of anti-IL-17A antibodies, we conducted animal experiments by measuring the IL-17A-induced Gro-α secretion in mouse sera[40]. We found a 9-fold increase in Gro-α levels in mouse sera collected 2 h after human IL-17A injection (1.5 mg/kg). 9NT IgG1 antibody (2 mg/kg) reduced the Gro-α level in mouse sera from 1574 $\pm$ 117 pg/mL to 650 $\pm$ 130 pg/mL, exhibiting a similar efficiency to that of the AIN457 antibody (Fig. 7B). Thus, the optimized antibody 9NT/S showed strong neutralization *in vitro* and *in vivo*.

4. Discussion

Phage display technology represents one of the most powerful tools for the production and selection of recombinant, fully human antibodies[18]. The advantages of phage-display antibody technology include a completely *in vitro* antibody selection process without mouse immunization, the rapid discovery of leading mAb candidates, less dependence on the complexity of antigens than other techniques, and a high throughput approach for screening mAbs[18]. Antibodies, especially those derived from IgM libraries, usually have low affinity for clinical applications[41]. To overcome this limitation, we need to perform affinity maturation to increase affinity, activity and bioactivity. In this study, we employed a strategy for parallelly mutating the VH and VL chains of the 7H9 scFv separately and subsequently combining optimized mutants. For this purpose, three different yeast libraries were generated and screened against antigens with decreasing concentrations using an equilibrium method. Although combining the affinity-improved VH and VL mutants might not produce binders with higher affinity as previously reported[42], the beneficial mutations in VH and VL mutants have a synergistic binding effect and thus ultimately result in increased affinity in most cases[32]. From the VHVL-Mut library, several affinity-improved clones were isolated. Compared with the original clone 7H9, the affinity-matured clone 8D3 showed an $\sim$233-fold increase in K_{off}, with an overall $\sim$8-fold improvement in K_D by Biacore. Furthermore, after analysis of these mutated residues, we found that three residues—L30G, H65N and H97D—in the CDR loops were predicted to be directly involved in antigen binding. In addition to antigen-binding regions, one mutation with a clear contribution to the affinity improvements, H93V, immediately follows the cysteine before the CDRH3 region and is sometimes used to identify the N-terminal residues on the CDRH3, which can affect loop conformation[43]. In this study, using the *in vitro* affinity maturation method, we improved the affinity of 7H9 and obtained the clone 8D3 with a slower off-rate, K_{off}. However, the Fab melting temperature (T_m) of 8D3 decreased to 59.4 °C, which is 7.4 °C lower than that of the original antibody 7H9 by DSC.

Several approaches have been reported to improve the thermalstability of antibodies[44]: *in vitro* evolution by grafting antigen-binding loops onto a framework with more favorable biophysical properties[23,35,36], combining random mutagenesis at elevated temperature[45], implementing consensus-based designs[46], disulfide bond engineering[47] and computational modeling[48]. Because the biophysical properties can be transferred between VH6 and VH3 formats[49], and because of the unstable nature of VH6/Vλ3, we used the CDR grafting approach to transfer the binding sites of 8D3 to the artificial human consensus framework of 4D5 to improve its properties in a straightforward manner. In this study, a structural model of 8D3 was generated by homology modeling. Compared to the structure of 4D5 (1PDB entry 1fvc), certain residues adjacent to the CDRs, as well as residues that may determine the conformation of the "outer loops" of upper core domains, were retained to preserve the topology of the potential antigen interaction surface. Moreover, residues L4, H6, H67 and H82, which are located inside the hybrid 4D5 framework, are critical for maintaining the framework structure. Structurally, these residues are buried directly underneath the CDRs or outer loops, inaccessible to protein antigens and are therefore not expected to affect immunogenicity. Our strategy proved to be successful. Incorporation of affinity-matured CDRs into the stabilized scaffold resulted in a highly stable, high-affinity antibody clone 9NT/S with a 1.7-fold higher K_D and an $\sim$17 °C higher Fab T_m than clone 8D3. The results are consistent with a previous report that mutations designed to stabilize antibodies can also lead to concomitant gains in affinity[45].

In the current study, all mature clones with improved affinity and thermostability exhibited enhanced neutralization potency against human IL-17A. In the neutralization assay, 8D3 displayed an $\sim$15-fold improvement in IC_{50} over 7H9, while 9NT and 9NS behaved similarly. However, we did not compare the IC_{50} values of these variants at the same time, and thus obtained different IC_{50} values for the reference AIN457. Relatively, 8D3 displayed an $\sim$2-fold higher IC_{50} than AIN457, while 9NT/S had an $\sim$1.5-fold lower IC_{50} than AIN457. In addition, the *in vivo* inhibitory activity

of 9NT was as potent as that of AIN457. Thus, 9NT/S was the best clone with superior affinity, thermostability and neutralization activity after rounds of optimization.

IL-17 is a proinflammatory cytokine involved in the progression of autoimmune diseases, such as rheumatoid arthritis and psoriasis, fibrotic diseases, chronic obstructive pulmonary diseases, and cancer, among others[1]. Targeting IL-17A offers an attractive treatment option for these diseases. Here, we implemented evolutionary approaches *in vitro* to discover and improve the biophysical properties of the fully human anti-IL-17A antibody 7H9. The affinity-matured and thermostability-improved antibody 9NT/S characterized in this study is a potential best-in-class candidate, either alone or in combination with other human inflammatory inhibitors, for IL-17A-related autoimmune diseases and cancer.

5. Conclusions

Antibodies are important tools for a broad range of applications because of their high specificity and ability to recognize target molecules. However, only a subset of antibodies possesses biophysical properties ideally suited for therapeutic or diagnostic antibodies. There is great demand for antibodies exhibiting affinity, stability, expression yield, resistance to aggregation and long half-life[22]. In the current study, we describe a novel fully human antibody against human IL-17A with high affinity, thermal stability and neutralization potency *in vitro* and *in vivo*. Specifically, we isolated a fully human antibody (7H9) with poor dissociation rate constant and thermostability from a large naïve phage-displayed scFv library. To improve its neutralization activity, we affinity-matured 7H9 through yeast-displayed random mutagenesis libraries. Moreover, the thermostability of this antibody was optimized through CDR grafting. As a result, the antibody 9NT/S against IL-17A might achieve superior therapeutic efficacy with a lower dose relative to AIN457. These approaches also have broad implications for the engineering of antibodies isolated from phage-displayed libraries.

Acknowledgments

This work was partially supported by National Key R&D Program of China under Grant 2017YFA0205400, National Natural Science Foundation of China under Grant 81874316, 81773781 and 81530093, National Drug Innovation Major Project of China under Grant 2018ZX09711001-003-001, Chinese Academy of Medical Sciences (CAMS, Beijing, China) Central Public-interest Scientific Institution Basal Research Fund under 2017PT31046 and 2018RC350004, CAMS Innovation Found for Medical Sciences (2016-I2M-3-008 and 2016-I2M-1-007).

Appendix A. Supporting information

Supporting data associated with this article can be found in the online version at https://doi.org/10.1016/j.apsb.2019.02.007.

References

1. Veldhoen M. Interleukin 17 is a chief orchestrator of immunity. *Nat Immunol* 2017;**18**:612–21.
2. Mi S, Li Z, Yang HZ, Liu H, Wang JP, Ma YG, et al. Blocking IL-17A promotes the resolution of pulmonary inflammation and fibrosis *via* TGF-β1-dependent and -independent mechanisms. *J Immunol* 2011;**187**:3003–14.
3. Zhang XW, Mi S, Li Z, Zhou JC, Xie J, Hua F, et al. Antagonism of Interleukin-17A ameliorates experimental hepatic fibrosis by restoring the IL-10/STAT3-suppressed autophagy in hepatocytes. *Oncotarget* 2017;**8**:9922–34.
4. Cui B, Cao X, Zou W, Wan Y, Wang N, Wang Y, et al. Regulation of immune-related diseases by multiple factors of chromatin, exosomes, microparticles, vaccines, oxidative stress, dormancy, protein quality control, inflammation and microenvironment: a meeting report of 2017 International Workshop of the Chinese Academy of Medical Sciences (CAMS) Initiative for Innovative Medicine on Tumor Immunology. *Acta Pharm Sin B* 2017;**7**:532–40.
5. Mease PJ, McInnes IB, Kirkham B, Kavanaugh A, Rahman P, van der Heijde D, et al. Secukinumab inhibition of interleukin-17A in patients with psoriatic arthritis. *N Engl J Med* 2015;**373**:1329–39.
6. Frieder J, Kivelevitch D, Menter A. Secukinumab: a review of the anti-IL-17A biologic for the treatment of psoriasis. *Ther Adv Chronic Dis* 2018;**9**:5–21.
7. Syed YY. Ixekizumab: a review in moderate to severe plaque psoriasis. *Am J Clin Dermatol* 2017;**18**:147–58.
8. Miossec P, Kolls JK. Targeting IL-17 and TH17 cells in chronic inflammation. *Nat Rev Drug Discov* 2012;**11**:763–76.
9. Wang EA, Suzuki E, Maverakis E, Adamopoulos IE. Targeting IL-17 in psoriatic arthritis. *Eur J Rheumatol* 2017;**4**:272–7.
10. Cui B, Eyers PA, Dobens LL, Tan NS, Mace PD, Link WA, et al. Highlights of the 2nd International Symposium on Tribbles and Diseases: tribbles tremble in therapeutics for immunity, metabolism, fundamental cell biology and cancer. *Acta Pharm Sin B* 2019;**9**:443–54.
11. Lerner RA. Combinatorial antibody libraries: new advances, new immunological insights. *Nat Rev Immunol* 2016;**16**:498–508.
12. Zhao C, Hu Z, Cui B. Recent advances in monoclonal antibody-based therapeutics. *Acta Pharm Sin* 2017;**52**:837–47.
13. Guan X. Cancer metastases: challenges and opportunities. *Acta Pharm Sin B* 2015;**5**:402–18.
14. Jiang W, Cai G, Hu PC, Wang Y. Personalized medicine in non-small cell lung cancer: a review from a pharmacogenomics perspective. *Acta Pharm Sin B* 2018;**8**:530–8.
15. Igawa T, Tsunoda H, Kuramochi T, Sampei Z, Ishii S, Hattori K. Engineering the variable region of therapeutic IgG antibodies. *MAbs* 2011;**3**:243–52.
16. Chao G, Lau WL, Hackel BJ, Sazinsky SL, Lippow SM, Wittrup KD. Isolating and engineering human antibodies using yeast surface display. *Nat Protoc* 2006;**1**:755–68.
17. Baker MP, Reynolds HM, Lumicisi B, Bryson CJ. Immunogenicity of protein therapeutics: the key causes, consequences and challenges. *Self Nonself* 2010;**1**:314–22.
18. Frenzel A, Schirrmann T, Hust M. Phage display-derived human antibodies in clinical development and therapy. *MAbs* 2016;**8**:1177–94.
19. Lonberg N. Fully human antibodies from transgenic mouse and phage display platforms. *Curr Opin Immunol* 2008;**20**:450–9.
20. Hou X, Hu Z, Cui B. Recent advances of phage display techniques for drug discovery. *Acta Pharm Sin* 2018;**53**:1279–88.
21. Bradbury AR, Marks JD. Antibodies from phage antibody libraries. *J Immunol Methods* 2004;**290**:29–49.
22. Ewert S, Huber T, Honegger A, Pluckthun A. Biophysical properties of human antibody variable domains. *J Mol Biol* 2003;**325**:531–53.
23. Ewert S, Honegger A, Pluckthun A. Stability improvement of antibodies for extracellular and intracellular applications: CDR grafting to stable frameworks and structure-based framework engineering. *Methods* 2004;**34**:184–99.
24. Sun W, Lin H, Hua F, Hu ZW. Optimizing the host bacteria to make a large naive phage antibody library in the recombination system. *Acta Pharm Sin* 2013;**48**:66–70.

25. Chen CG, Fabri LJ, Wilson MJ, Panousis C. One-step zero-background IgG reformatting of phage-displayed antibody fragments enabling rapid and high-throughput lead identification. *Nucleic Acids Res* 2014;**42**:e26.
26. Ferreira MU, Katzin AM. The assessment of antibody affinity distribution by thiocyanate elution: a simple dose-response approach. *J Immunol Methods* 1995;**187**:297–305.
27. Garber E, Demarest SJ. A broad range of Fab stabilities within a host of therapeutic IgGs. *Biochem Biophys Res Commun* 2007;**355**:751–7.
28. Sblattero D, Bradbury A. Exploiting recombination in single bacteria to make large phage antibody libraries. *Nat Biotechnol* 2000;**18**:75–80.
29. Silacci M, Lembke W, Woods R, Attinger-Toller I, Baenziger-Tobler N, Batey S, et al. Discovery and characterization of COVA322, a clinical-stage bispecific TNF/IL-17A inhibitor for the treatment of inflammatory diseases. *MAbs* 2016;**8**:141–9.
30. Pullen GR, Fitzgerald MG, Hosking CS. Antibody avidity determination by ELISA using thiocyanate elution. *J Immunol Methods* 1986;**86**:83–7.
31. Bottermann M, Lode HE, Watkinson RE, Foss S, Sandlie I, Andersen JT, et al. Antibody-antigen kinetics constrain intracellular humoral immunity. *Sci Rep* 2016;**6**:37457.
32. Wang Y, Keck ZY, Saha A, Xia J, Conrad F, Lou J, et al. Affinity maturation to improve human monoclonal antibody neutralization potency and breadth against hepatitis C virus. *J Biol Chem* 2011;**286**:44218–33.
33. Sela-Culang I, Kunik V, Ofran Y. The structural basis of antibody-antigen recognition. *Front Immunol* 2013;**4**:302.
34. Kawa S, Onda M, Ho M, Kreitman RJ, Bera TK, Pastan I. The improvement of an anti-CD22 immunotoxin: conversion to single-chain and disulfide stabilized form and affinity maturation by alanine scan. *MAbs* 2011;**3**:479–86.
35. Jung S, Pluckthun A. Improving *in vivo* folding and stability of a single-chain Fv antibody fragment by loop grafting. *Protein Eng* 1997;**10**:959–66.
36. Willuda J, Honegger A, Waibel R, Schubiger PA, Stahel R, Zangemeister-Wittke U, et al. High thermal stability is essential for tumor targeting of antibody fragments: engineering of a humanized anti-epithelial glycoprotein-2 (epithelial cell adhesion molecule) single-chain Fv fragment. *Cancer Res* 1999;**59**:5758–67.
37. Lee CV, Liang WC, Dennis MS, Eigenbrot C, Sidhu SS, Fuh G. High-affinity human antibodies from phage-displayed synthetic Fab libraries with a single framework scaffold. *J Mol Biol* 2004;**340**:1073–93.
38. Holm L, Sander C. The FSSP database: fold classification based on structure-structure alignment of proteins. *Nucleic Acids Res* 1996;**24**:206–9.
39. Weitzner BD, Jeliazkov JR, Lyskov S, Marze N, Kuroda D, Frick R, et al. Modeling and docking of antibody structures with Rosetta. *Nat Protoc* 2017;**12**:401–16.
40. Zaretsky M, Etzyoni R, Kaye J, Sklair-Tavron L, Aharoni A. Directed evolution of a soluble human IL-17A receptor for the inhibition of psoriasis plaque formation in a mouse model. *Chem Biol* 2013;**20**:202–11.
41. Eisen HN. Affinity enhancement of antibodies: how low-affinity antibodies produced early in immune responses are followed by high-affinity antibodies later and in memory B-cell responses. *Cancer Immunol Res* 2014;**2**:381–92.
42. Schier R, McCall A, Adams GP, Marshall KW, Merritt H, Yim M, et al. Isolation of picomolar affinity anti-c-erbB-2 single-chain Fv by molecular evolution of the complementarity determining regions in the center of the antibody binding site. *J Mol Biol* 1996;**263**:551–67.
43. North B, Lehmann A, Dunbrack Jr. RL. A new clustering of antibody CDR loop conformations. *J Mol Biol* 2011;**406**:228–56.
44. McConnell AD, Zhang X, Macomber JL, Chau B, Sheffer JC, Rahmanian S, et al. A general approach to antibody thermostabilization. *MAbs* 2014;**6**:1274–82.
45. Jung S, Honegger A, Pluckthun A. Selection for improved protein stability by phage display. *J Mol Biol* 1999;**294**:163–80.
46. Steipe B. Consensus-based engineering of protein stability: from intrabodies to thermostable enzymes. *Methods Enzymol* 2004;**388**:176–86.
47. Gong R, Vu BK, Feng Y, Prieto DA, Dyba MA, Walsh JD, et al. Engineered human antibody constant domains with increased stability. *J Biol Chem* 2009;**284**:14203–10.
48. Chennamsetty N, Voynov V, Kayser V, Helk B, Trout BL. Design of therapeutic proteins with enhanced stability. *Proc Natl Acad Sci U S A* 2009;**106**:11937–42.
49. Schaefer JV, Pluckthun A. Transfer of engineered biophysical properties between different antibody formats and expression systems. *Protein Eng Des Sel* 2012;**25**:485–506.